International Journal of Non–Linear Mechanics 161 (2024) 104670

Contents lists available at ScienceDirect

International Journal of Non-Linear Mechanics

journal homepage: www.elsevier.com/locate/nlm

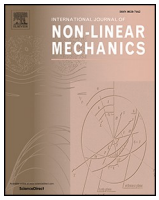

An approach to the micro-strain distribution inside nanoparticle structure

A.S. Abdel-Rahman [a,*], Youssef A. Sabry [b]

[a] Physics Department, Faculty of Science, Cairo University, Egypt
[b] Abul-Houl Academy, College of Mathematics, Egypt

ARTICLE INFO

Keywords:
Nanostructure
Microstuctural models
Strain
Crystalline size
Williamson-Hall
Scherrer's equation

ABSTRACT

Williamson-Hall, Stocks-Wilson, Scherrer, Halder-Wagner, and Size-Strain Plot (SSP) methods are used essentially to ensure the material particle size falls at the nano-level. They treat the broadening in the XRD peak as a sum of Gauss and Lorentz diffraction probability functions. In this work, an approach to the microstrain distribution is presented as a strain distribution (SD) model, assuming a nanostructure as a liquid drop where surface tension controls the particle positions while strain controls the geometry and spacing of the lattice parameters. The number of diffraction planes is considered in the model, treated as a Gaussian-like (or Lorentzian-like) function, and estimated with numerical analysis. The SD model writes an equation about the broadening, peak position, and lattice parameters to estimate the crystalline size and strain exponent. Williamson-Hall, Stocks-Wilson, and Scherrer can be explained as approximations for this model, and the presence of negative strain is explained. Possible approximations can show Halder-Wagner and SSP as another face of the SD model equation. The strain exponent, which is estimated here, is more useful than the average micro-strain, which is obtained from previous models. The strain exponent role in the nanoparticle reactions with materials can be discussed and explained. The change in crystal system as bulk material is reduced to nanostructure can be negated according to the SD model.

1. Introduction

Nanoparticles, in the dimensions of 1–100 nm, possess many unique size-dependent physical and chemical properties different from their bulk counterparts [1]. It is reported that elastic properties are one of the most important physical properties, the tuning of which can modify many physical properties such as optical, electrical, surface, etc. Because of this, many nanoparticles find enormous application in different branches of science, such as optoelectronic devices [2], light-emitting diodes [3,4], solar cells [5,6], and drug-delivery applications [7]. Many scientists show the effect of reducing the bulk material to micro- and nanostructure on the electrical, optical, thermal, etc. properties of nanoparticles where the material shows enormous and more useful properties [8,9].

Explicit modelling of nanostructures is necessary for tailoring the material to have specific features. Considering the strain inside the nanoparticle is the major issue that changes the point of view to the unique properties of the material on the nanoscale. The distribution of this strain inside the nanostructure is not well defined. Most current models consider the average strain and deal with the X-ray diffraction (XRD) structure factor as the main reason for diffraction peak broadening.

Diffraction-peak broadening shows information about nanostructural parameters; particularly lattice strains and the sizes of incoherently diffracting domains. Three major suggestions [10] have been made to characterize the diffraction-peak broadening: (i) The crystal is broken into "crystallites" so small (10^{-5} to 10^{-8} cm in dimensions) that diffraction broadening occurs; (ii) the crystal is broken into small crystals with different mean lattice parameters; and (iii) the broadening was due to distortion of fairly large crystals ($\sim 10^{-4}$ cm in linear dimensions).

To produce a physical specimen that is broadening-free, all effects, especially instrumental ones, must be removed. It is worthwhile to study the applicability of preset peak-shape functions in the size-strain analysis because of the great interest there is in accurately modelling peak broadening in the [11–13] analysis in terms of physical (size and strain) parameters [14–16]. Moreover, the results obtained by the integral-breadth and/or Warren-Averbach analyses were usually not comparable. The integral-breadth method gives volume-weighted domain sizes and an upper limit on strain. The Warren-Averbach analysis shows large surface-weighted domain sizes while a mean-square

* Corresponding author.
E-mail address: asabry@sci.cu.edu.eg (A.S. Abdel-Rahman).

https://doi.org/10.1016/j.ijnonlinmec.2024.104670
Received 4 August 2023; Received in revised form 2 December 2023; Accepted 6 February 2024
Available online 7 February 2024

strain averages over some distance perpendicular to the diffracting planes.

Although the instrumental errors come from many issues, they are decreased as possible in these models (Scherrer [17–19], Stokes-Wilson [20], Williamson-Hall [21,22], Halder-Wagner [23–25], SSP [26–28], and strain-distribution (SD) which presented in this work) as follows:

Scherrer's equation is derived directly from the XRD scattering structure factor without taking instrumental errors into account. Many scientists directly use this equation for the intensive peak of the XRD pattern. So they estimate the full width at the half maximum of the diffraction peak profile FWHM, or w, and thus high errors will be incorporated into the results. Other scientists use average crystalline size to reduce errors. The more accurate method is taking the slope of the best linear fit of the $(1/w)$-cosθ plot.

Other models use the linear fit of their plots to reduce the errors; in this work, the SD model also uses the plot in Figs. 7 and 8 to reduce the instrumentation errors.

Many studies on nanoparticle size and strain determinations using the various methods above were reported. Each method sets a relation between diffraction angle and FWHM, and then the determination of crystallite size and micro-strain is applicable. In all of the previous methods, the Miller indices did not appear directly in their equations, even though they were taken into account at the peak position.

To simplify the material representations, models and simulations are built to study the physical conditions and predict the particular constraints of the situation. This reflects the importance of physical models and theoretical approaches in material science. The widespread use of nanostructures in our society has increased interest in studying and modelling nanoscale materials, as well as adapting these materials to our needs.

This work aims to study more thoroughly the source of broadening from another point of view: the diffraction peak in the 3D nanostructure, the micro-strain inside the nanoparticle, and the number of diffraction planes. In this article, a new model for nanostructure is introduced and how it is formed. The faults of the previous models, such as negative strain, are explained by this theoretical approach. Drawing the strain inside the nanoparticle is possible here, where previous models only showed an average strain, which is not enough for our needs. The strain exponent role is a major factor that can explain the reaction of the nanoparticles with materials. The application of the SD model is important for vibration [29–31], of molecules [32], internal friction [33–36], and other point physical problems [37–42].

2. Methodology

This study will consider a spherically shaped aggregate in nanoparticle size of single-phase crystal lattices; they are accumulated to be like a liquid drop. The more general case can be investigated with an ellipsoidal structure in the future. There are three micro-strains [43] (ε_a, ε_b, and ε_c) that cause the perfect lattices to be compressed non-uniformly (due to different lattice parameters) to change the periodic uniform structure lattice parameters and orientations in 3D to draw a spherical shape; this strain works like surface tension in liquid drops.

This work shows the effect of curvature strain due to the wrapping of material crystals to form nanoparticles (which will be explained in detail in Section 2.2). There are different strains, such as thermal, tensile, shear, normal, etc., that also affect the nanostructure, but their effects are almost equally felt on all crystals inside the nanostructure. The curvature strain (from here and later, "strain" only) is taken as the major factor that shows the broadening of XRD peaks.

According to these assumptions, one can predict that the perfect crystal lattice (without strain) will hold the center of the nanoparticle sphere ($x = 0$; x is the displacement vector from the center of the sphere to its surface) and give the central diffraction peak line (d_1 in Fig. 1). From the center to the surface of the sphere, the stress (or the strain ε [44]) grows up (slight change in the interplanar distance in d_2) to reach

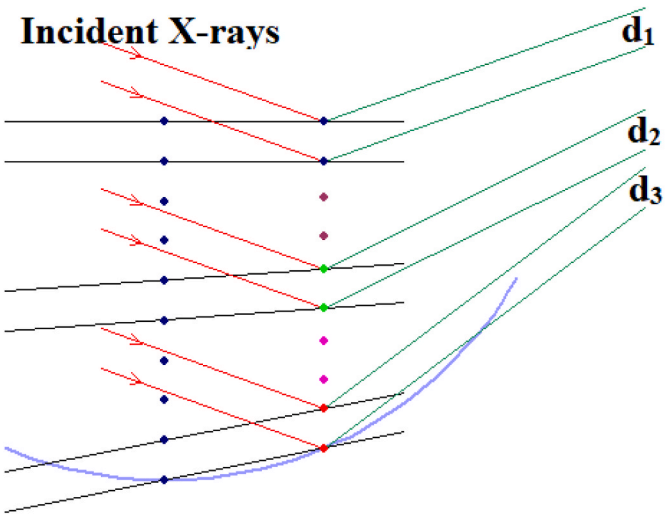

Fig. 1. Micro-strain effect in the nanoparticle.

the surface at maximum strain (ε_{max}) at $x = D/2$, where D is the crystallite size. The peak is broadening due to the much larger change in the interplanar distances (from d_1 to d_3).

Bragg's diffraction is the major factor in X-ray diffraction and is written in direct space as:

$$2d_0 \cdot Sin\ \theta_0 = n\lambda \tag{1}$$

where d_0 is the interplanar spacing of Miller indices hkl at the center of the diffraction peak with angle θ_0, the diffraction angle is denoted by 0 to be distinguished from the un-denoted angle that stands for variation angle about the peak center, and from here and over, the first order of diffraction will be considered ($n = 1$).

2.1. Peak profile (probability regime)

The diffraction peak profiles are treated as the sum of Gaussian G and Lorentzian L profiles (a pseudo-Voigt profile may also be introduced, but the same results were obtained); this treatment is also used in X-ray fluorescence XRF in Ref. [45]. These profiles are probability distribution functions that characterize the probability of diffraction on a specific plane. Both G and L functions can be expressed in terms of FWHM (w in radians) as follows [46,47]:

$$G = A\cdot\exp\left(-\frac{(\theta-\theta_0)^2}{w^2}\ln(16)\right)$$
$$L = B\left[\frac{w^2}{4(\theta-\theta_0)^2+w^2}\right] \tag{2}$$

where A and B represent the peak amplitudes in each profile. In both of these functions, the intensity falls to their half value when θ_f-$\theta_0 = w/2$. They share the same profile and FWHM but differ in the tail shape, where the Lorentzian profile has a longer tail than the Gaussian and approaches zero slower, as shown in Fig. 2.

The differentiation of each function according to the angle θ will be:

$$\frac{dG}{d\theta} = G'(\theta) = -2A\frac{(\theta-\theta_0)}{w^2}\ln(16)\exp\left(-\frac{(\theta-\theta_0)^2}{w^2}\ln(16)\right) =$$
$$-2\ln(16)\frac{(\theta-\theta_0)}{w^2}G \tag{3}$$

$$\frac{dL}{d\theta} = L'(\theta) = -8B(\theta-\theta_0)\frac{w^2}{\left(4(\theta-\theta_0)^2+w^2\right)^2} = -8\frac{(\theta-\theta_0)}{\left(4(\theta-\theta_0)^2+w^2\right)}L \tag{4}$$

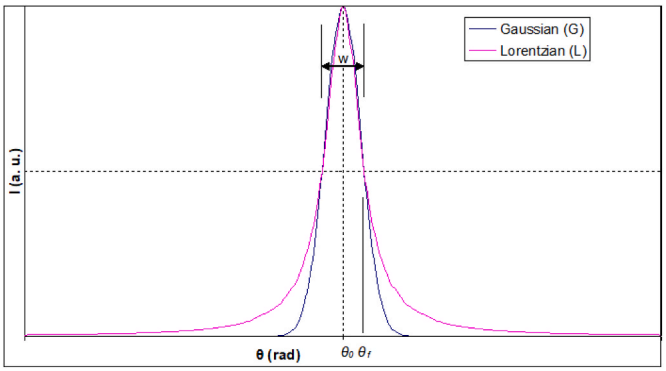

Fig. 2. Gaussian and Lorentzian profiles.

One can try:

$$\left.\frac{dG}{d\theta}\right|_{\theta_0}^{\theta_f} \approx \left.\frac{\Delta G}{\Delta\theta}\right|_{\theta_0}^{\theta_f} = \frac{A - \frac{1}{2}A}{\theta_0 - \theta_f} = -\frac{\frac{1}{2}A}{\frac{1}{2}w} = -\frac{A}{w} \tag{5}$$

Also, the same result will be found for Lorentz; the left-hand side of Eqs. (3) and (4) at θ_f will be:

$$G'(\theta_f) = -2\ln(16)\frac{\frac{1}{2}w}{w^2}\frac{1}{2}A = -\ln(4)\frac{A}{w} \quad L'(\theta_f) = -\frac{B}{w} \tag{6}$$

If it is difficult to calculate the derivative of a function like a Gauss or Lorentz profile, it is possible to replace its derivative at FWHM by its amplitude value multiplied by Q/w, where the factor Q has a range from 1 to 1.3863 (=ln(4)).

2.2. Micro-strain

One can assume an ellipsoid structure, and so the three strains (ε_a, ε_b, and ε_c) are different, but in this work, the spherical shape will be introduced. In 2D, the strain ε_a is zero along the x-axis, and ε_b is zero along the y-axis. As one moves away from the major axis, strain increases (causing the lattice lengths to decrease) to reach ε_{max} on the surface of the sphere. The value of ε_{max} is direction-independent, where all strains regardless of their directions should be equal (i.e., ε_{max}) at $D/2$.

Fig. 3 shows a quartile of the nanoparticle (2-dimensional projection). Behind the vertical and horizontal curves (parabolas) are the strain functions (functions in displacement), and the intercepts of these lines represent the location of the atoms. The last vertical arc is the circular surface of the nanoparticle.

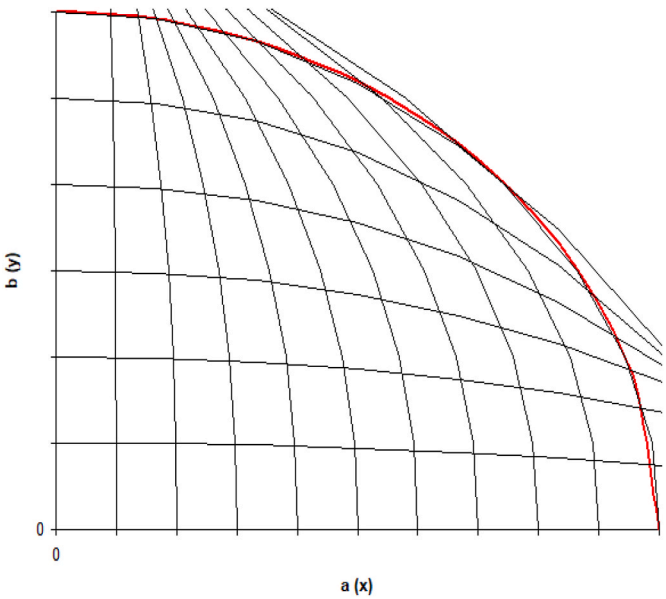

Fig. 3. Quartile of the nanoparticle 2D projection with micro-strain functions.

According to the circle equation $x^2+y^2=(D/2)^2$, the definition of the compression strain in the x-direction is [48]:

$$\varepsilon = -\frac{\Delta x}{x} = \frac{x_0 - x}{x_0} \tag{7}$$

where x_0 is the original location of the subject and x is that location after compression, the maximum strain in the x-direction can be found at $x_0 = D/2$. Then the strained location of the subject will be written in terms of maximum strain in the x-direction as:

$$x = \frac{D}{2}\left(1 - \varepsilon_x^{\max}\right) \tag{8}$$

This value is y-dependent and can be substituted in a circle equation to find a relation for the maximum strain in the x-direction in terms of the y-axis value as follows:

$$\varepsilon_x^{\max}(y) = 1 - \sqrt{1 - \left(\frac{y}{D/2}\right)^2} \tag{9}$$

Since the maximal strain occurs when both x and y values equal $\frac{D/2}{\sqrt{2}}$, this strain value should be 0.293. In the case of 3D, the x-axis strain equation will take the form:

$$\varepsilon_x^{\max}(y,z) = 1 - \sqrt{1 - \left(\frac{y}{D/2}\right)^2 - \left(\frac{z}{D/2}\right)^2} \tag{10}$$

and the maximal strain should be 0.423 as calculated for the isotropic sphere (this value is very large and the infinitesimal strains should be lower), while the x, y, and z values equal $\frac{D/2}{\sqrt{3}}$.

In Fig. 3, one can notice the change of cubic structure into orthorhombic or tetragonal structures; this was noticed recently in nanoparticles of gold [49], where it differs from the usual face-centered cubic bulk structure of gold. Due to the overlap of XRD diffractions of these structures, one can predict the change of crystal structure to another point group in the nanostructure. The appropriate expression to describe this issue is not to consider a change in crystal structure but rather a strained crystal nanostructure.

To describe the strain function (vertical parabolas intercepting the x-axis at integer multipliers of a), one can estimate the gradient of the strain function curvature on the basis of very small strains. The change of strain from Eq. (7) is:

$$\varepsilon = \frac{dx}{x} \quad and \quad d\varepsilon = -\frac{d(dx)}{x} + \frac{(dx)^2}{x^2} \approx \varepsilon^2 \tag{11}$$

According to the derivations of the Extended Mooney-Rivlin model for neo-Hookean solids [48], the behaviour of small strains before the critical elongation suggests the change of strain is inversely proportional to the displacement x; hence, Equ. 11 can be corrected to:

$$d\varepsilon = A\frac{\varepsilon^2}{x} \quad or \quad \frac{d\varepsilon}{\varepsilon} = A\frac{dx}{x^2} \tag{12}$$

Integration of Equ. 12 and applying the boundary condition ($x \to D/2 \quad \varepsilon \to \varepsilon_{\max}$) to the micro-strain equation can be written as follows:

$$\varepsilon_x = \varepsilon_{\max}\exp\left(-c\left(\frac{D/2}{x} - 1\right)\right) \tag{13}$$

While c is constant, it represents the growth of the strain from the center of the sphere to its surface and will be called the strain exponent.

The reciprocal space will be introduced, and all asterisked terms will

be reciprocals and related to the direct term inversely. The reciprocal strain function may be written as:

$$\varepsilon* = \varepsilon_{\max} * \exp\left(c\left(\frac{Dx*}{2} - 1\right)\right) \tag{14}$$

The summation of strains in any direction, one over the other, will reduce the whole nanoparticle's dimensions to a sphere's radius, so one can write:

$$m_a a(1-\varepsilon_{\max}) = m_b b(1-\varepsilon_{\max}) = m_c c(1-\varepsilon_{\max}) = \frac{D}{2} \tag{15}$$

where m_a, m_b, and m_c are the number of atoms in each direction from the center of the sphere to its surface, the maximum strain can also be expressed in terms of these numbers:

$$\varepsilon_{\max} \approx m_a\varepsilon_a = m_b\varepsilon_b = m_c\varepsilon_c \tag{16}$$

and so one can write them in reciprocal space as:

$$\frac{a*}{\varepsilon_a*} = \frac{b*}{\varepsilon_b*} = \frac{c*}{\varepsilon_c*} \approx \frac{x*}{\varepsilon*} \tag{17}$$

This equation illustrates the ratio of longitudinal to transverse strain, with the longest lattice parameters meeting the highest strain, so all lattice directions reach the nanoparticle surface on one foot.

2.3. Interplanar distance

In this work, the change of lattice angles with strains is neglected (this assumption was verified by applying the model to different lattice systems, which showed the validity of the SD model), so the general form of lattices that can be studied is the orthorhombic lattice, and the reciprocal interplanar distance can be written as follows:

$$d_0* = \sqrt{h^2a*^2 + k^2b*^2 + l^2c*^2} \tag{18}$$

and the strained interplanar distance is

$$d* = \sqrt{\frac{h^2}{a^2\left(1-\frac{x*}{\varepsilon*}a\right)^2} + \frac{k^2}{b^2\left(1-\frac{x*}{\varepsilon*}b\right)^2} + \frac{l^2}{c^2\left(1-\frac{x*}{\varepsilon*}c\right)^2}} \tag{19}$$

The derivation of the term (x^*/ε^*) which respect to x^* is:

$$\frac{d}{dx*}\left(\frac{x*}{\varepsilon*}\right) = \frac{1}{\varepsilon*}\left(1 - c(D/2)\frac{x*}{\varepsilon*}\right) \tag{20}$$

The derivation of the reciprocal interplanar distance with respect to the reciprocal displacement vector (instead of the strain) is approximated to be:

$$\frac{\partial d*}{\partial x*} \approx \frac{1}{d_0 * \varepsilon*}\left[1 - c(D/2)\frac{x*}{\varepsilon*}\right]\left[\frac{h^2}{a} + \frac{k^2}{b} + \frac{l^2}{c}\right] \tag{21}$$

2.4. Number of diffraction planes

The diffraction intensity is directly proportional to the number of diffraction planes (N). According to this main assumption, as one moves away from the center of the nanoparticle, the strain grows, the lattice parameters decrease, and hence the interplanar distances decrease. So it is more suitable to study the variation of the number of diffraction planes with the diffraction angle. The definition of the number of diffraction planes may be clear from Fig. 4, which illustrates the d_{21} and its relation to the displacement in $2D$.

As shown in Fig. 4, the number of interplanar distances is defined as the ratio between the displacement and the interplanar distance projection on this displacement and may be written in 3D as follows:

$$N_m = \frac{\sqrt{(x_{m+1}-x_m)^2 + (y_{m+1}-y_m)^2 + (z_{m+1}-z_m)^2}}{d_m \cos\varphi} \tag{22}$$

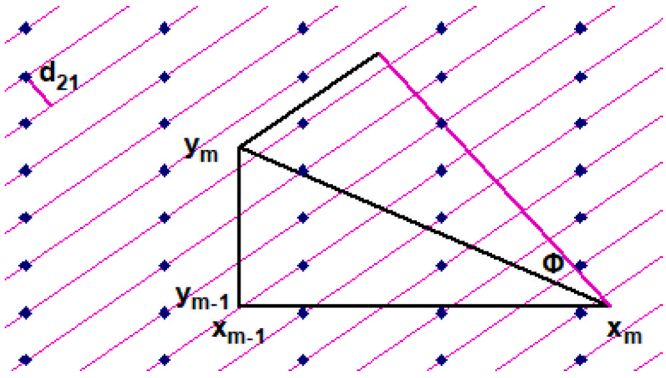

Fig. 4. The interplanar distance d_{21} and displacement vector in 2D.

In this work, the displacement x_m is arbitrary inside the nanoparticle, so it is chosen in the x-direction only and parallel to the interplanar distance. where m is an integer that represents the step number in which interplanar distance appears constant; $m = 0$ represents the N_0 region (maximum intensity); as m increases, the number of interplanar distances decreases. where m_∞ is the maximal value of m, which happens at the surface of the particle, and typically m_∞ has a large value, such as thousands (by assuming the lattice parameter is in the range of a few angstroms and the crystalline size D is about 100 nm), where the ratio between the particle size and the used wavelength is in the order of 10^3. Then the number of d-planes is:

$$\begin{aligned} N_m &= \frac{(x_{m+1}-x_m)}{d_m} \approx \frac{1}{d_0(1-\varepsilon_m)}\left[(m+1)a(1-\varepsilon_{m+1}) - ma(1-\varepsilon_m)\right] \\ &= \frac{a}{d_0(1-\varepsilon_m)}\left[1 + m(\varepsilon_m - \varepsilon_{m+1}) - \varepsilon_{m+1}\right] \end{aligned} \tag{23}$$

One can estimate the displacement x_f at FWHM, where the number of d-planes is reduced to its half value.

2.5. Numerical analysis

The number of interplanar distances is calculated based on Eq. (23) for different values of c, $D/2$, a, and d_0 to investigate the profile of N regarding the displacement integer m. Fig. 5 shows this profile with some selected values of c. The full numeric data is presented in the supplementary document.

The values of $c < 0.6$ cannot be considered for variation in the number of interplanar distances due to their unacceptable shape. The profile shown is similar to that of Gauss and Lorentz, but it is built on the effect of strain on the interplanar distances. Eq. (23) can be considered as a XRD peak profile, and the upcoming results are based on it. This numeric analysis will also benefit the approximation and correlation of terms, which will be discussed in the next section.

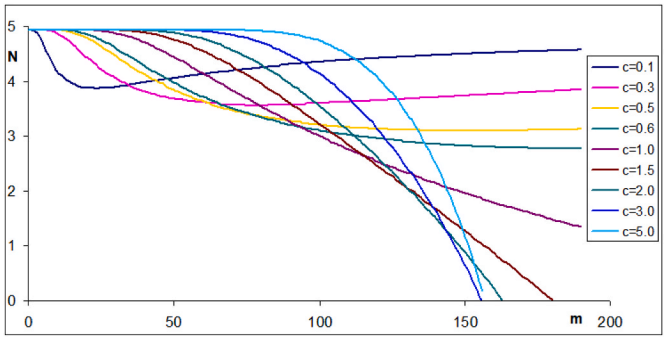

Fig. 5. The number of the interplanar distances N and displacement integer m.

3. Results and discussion

3.1. General formula

Since the number of d-planes has the same profile as Gauss/Lorentz and the differentiation of Eq. (23) is too complicated, one can predict:

$$\left.\frac{\partial N}{\partial x*}\right|_{x_0*}^{x_f*} = \frac{1}{Q}\cdot\frac{N_0 - ½N_0}{(sd_0* - x_f*)} = \frac{1}{Q}\cdot\frac{N_0}{2(sd_0* - x_f*)} \tag{24}$$

The number of d-planes at the center of the sphere is N_0 and corresponds to $x_0 = 0$, and this cannot be used for $x^*(=\infty)$, so one can approximate it to sd_0^*, where s is a constant.

The micro-strain that happens inside the nanoparticles is the major factor affecting Bragg's diffraction, where the interplanar spacing and diffraction angle are functions of this strain, so the derivation of Bragg's equation in reciprocal space may be written as follows:

$$\frac{\partial d*}{\partial\theta} = \frac{2}{\lambda}Cos\ \theta \tag{25}$$

To study the diffraction peak and its broadening, the variation of the number of diffraction planes (which represents intensity) to the diffraction angle may be written by the chain rule as follows:

$$\frac{\partial N}{\partial\theta} = \frac{\partial N}{\partial x*}\cdot\frac{\partial x*}{\partial d*}\cdot\frac{\partial d*}{\partial\theta} = \frac{\partial N}{\partial x*}\cdot\frac{1}{\partial d*/\partial x*}\cdot\frac{\partial d*}{\partial\theta} \tag{26}$$

and at FWHM, the left-hand side term in Eq. (26) can be written as follows:

$$\left.\frac{\partial N}{\partial\theta}\right|_{\theta_0}^{\theta_f} = \frac{1}{Q}\cdot\frac{N_0 - ½N_0}{\theta_0 - \theta_f} = -\frac{1}{Q}\cdot\frac{N_0}{w} \tag{27}$$

By introducing equations (21), (24), (25) and (27) at FWHM, equation (26) can be rewritten as:

$$w\cos\theta_f = \frac{2}{\varepsilon_f*}\left[1 - c(D/2)\frac{x_f*}{\varepsilon_f*}\right]\ \frac{1}{d_0*}\left[\frac{h^2}{a} + \frac{k^2}{b} + \frac{l^2}{c}\right](\lambda x_f* - 2s\sin\theta_0) \tag{28}$$

This equation is very similar to those of Williamson-Hall, Scherrer, and Stokes-Wilson by approximating the FWHM angle θ_f to the diffraction angle θ_0 and assuming both $\frac{1}{d_0*}\left[\frac{h^2}{a} + \frac{k^2}{b} + \frac{l^2}{c}\right]$ and x_f* terms are constants:

$$w\cos\theta_0 = \frac{K\lambda}{D} + 4\varepsilon\sin\theta_0 \tag{29}$$

The relation between $w\cos\theta_0$ and $\sin\theta_0$ should be linear, and the slope is wavelength-independent, as expected by Stokes, while the interception is typical of Scherrer's equation.

Another important issue is the negative sign in the $\sin\theta_0$ term. Articles such as [50,51] notice the negative microstrain (slope in Williamson-Hall), which is physically meaningless. The negative micro-strain here can be attributed to the approximations in the Williamson-Hall method, and its plot results in very scattering points, as discussed in Ref. [45].

Upon this comparison, one can predict that Williamson-Hall, Scherrer, and Stokes-Wilson are approximations of what is driven in this work. Since x_f* is the displacement inside the nanoparticle where the number of d-planes is reduced to half, this term is not constant and depends on the broadening w as follows:

$$x_f* = \frac{k}{w} \tag{30}$$

where k is constant, another issue; the cosine of the angle θ_f in Eq. (28) can be written as:

$$\cos\theta_f = \cos\left(\theta_0 + \frac{w}{2}\right) \approx \cos\theta_0 - \frac{w}{2}\sin\theta_0 \tag{31}$$

This methodology results in another modification to Eq. (28) to be a strain-distribution (SD) model inside nanostructures and will be written as:

$$\frac{w^2\left(\cos\theta_0 - \frac{w}{2}\sin\theta_0\right)}{d_0\left[\frac{h^2}{a} + \frac{k^2}{b} + \frac{l^2}{c}\right]} = \frac{2}{\varepsilon_f*}\left[1 - c(D/2)\frac{x_f*}{\varepsilon_f*}\right](\lambda k - 2s(w\sin\theta_0)) \tag{32}$$

One can notice a similar form between this equation and the Halder-Wagner and SSP methods by the appearance of broadening in square form. To verify the deduced model by applying it to different lattice systems, six real XRD patterns for CuO [45], $LaFeO_3$ [13], Mn_3O_4 [52], Fe_2O_3 [53], ZnO [54], and MgO [55] were used. Fig. 6 shows the XRD patterns for theses samples.

The SD model (Eq. (32)) was used to plot the relation between $\frac{w^2\left(\cos\theta_0 - \frac{w}{2}\sin\theta_0\right)}{d_0\left[\frac{h^2}{a} + \frac{k^2}{b} + \frac{l^2}{c}\right]}$ and $w\sin\theta_0$ and is presented in Figs. 7 and 8 for different lattice systems, as explained in Table 1. They show a linear dependence as predicted by the model, and the error bars are used to reduce the calculation errors as much as possible.

According to the above data, the model has been successfully applied to all crystal systems, and although the Williamson-Hall strain is positive in all systems, the relationships in the figures have negative slopes, and the positional intercepts are consistent with Eq. (32).

3.2. Crystalline size and strain exponent

According to Eq. (32), both slope and intercept are functions in c and D; by using the numeric data, the term $\frac{2}{\varepsilon_f*}\left[1 - c(D/2)\frac{x_f*}{\varepsilon_f*}\right]$ was plotted against the constant c and seems to be in an inverse relationship after $c > 0.6$, as shown in Fig. 9.

This term is correlated and multiplied by the constant s, which is found at an average of 0.005. By introducing the average value of broadening $w_{av} = 0.008$ rad, one can estimate the correlation between the term $\frac{2x_f*}{\varepsilon_f*}\left[1 - c(D/2)\frac{x_f*}{\varepsilon_f*}\right]$ and $D/2$ (Fig. 10).

Thus, Eq. (32) can finally be written in its approximate form:

$$\frac{w^2\left(\cos\theta_0 - \frac{w}{2}\sin\theta_0\right)}{d_0\left[\frac{h^2}{a} + \frac{k^2}{b} + \frac{l^2}{c}\right]} = \frac{4\times10^{-3}}{D}\lambda - \frac{3.1\times10^{-3}}{c}(w\sin\theta_0) \tag{33}$$

This equation was applied to Table 1 to compare the SD model results with what had been estimated before. The obtained results are listed in Table 2 beside the percentage errors between the SD model and previous models. The large errors may be attributed to the large values of the micro-strains. This is also noticed as a relatively high difference between the XRD peak broadening crystalline size and that obtained from the scanning electron microscope (SEM) in Ref. [56].

Eq. (33) may be approximated to this formula in order to facilitate its

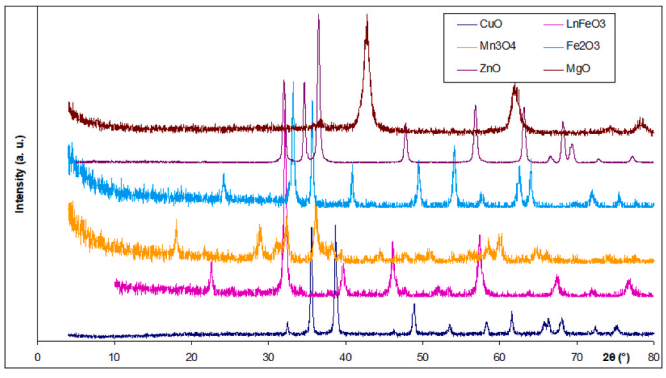

Fig. 6. XRD patterns of the six samples used for verification.

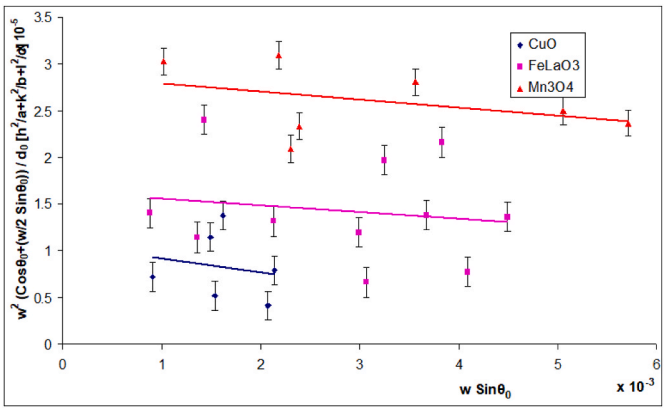

Fig. 7. SD model application on CuO, $FeLaO_3$, and Mn_3O_4 nanoparticles.

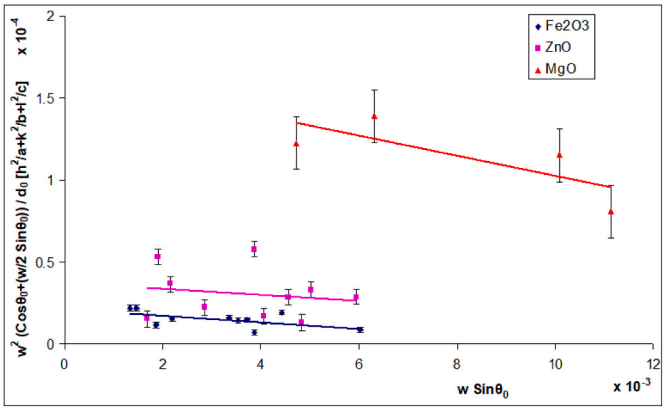

Fig. 8. SD model application on Fe_2O_3, ZnO, and MgO nanoparticles.

Table 1
Application of SD model to many lattice systems.

Material	Lattice	Space group	Slope (× 10^{-3})	Interception (× 10^{-5})
CuO	Monoclinic	C2/c [15]	−1.48	1.45
$LaFeO_3$	Orthorhombic	Pnma [62]	−0.72	1.53
Mn_3O_4	Tetragonal	$I4_1/amd$ [141]	−0.86	2.87
Fe_2O_3	Trigonal	R $\bar{3}$ c [167]	−1.98	2.14
ZnO	Hexagonal	P6mm [183]	−1.76	3.71
MgO	Cubic	Fm $\bar{3}$ m [225]	−6.22	17.75

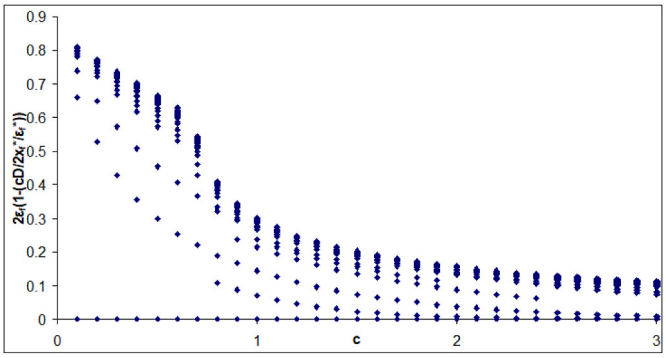

Fig. 9. Term correlation with strain exponent *c*.

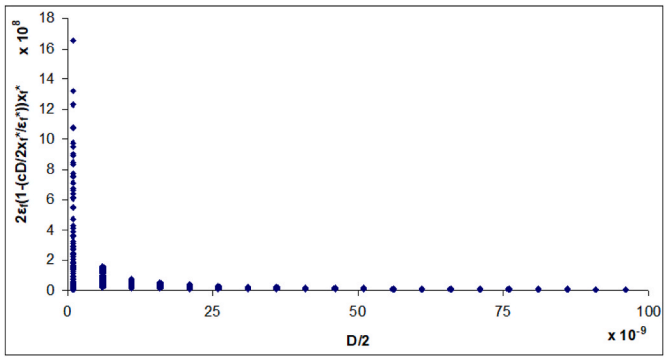

Fig. 10. Term correlation with half-crystalline size *D/2*.

Table 2
Obtained results from the SD model.

Material	D[a] (nm)	ε[a] (× 10^{-3})	D (nm)	Error (%)	c
CuO	44.79	0.84	42.4	5.34	2.09
$LaFeO_3$	38.71	1.26	40.1	3.59	4.28
Mn_3O_4	30.74	2.49	21.4	30.38	3.62
Fe_2O_3	34.87	1.78	28.7	17.69	1.56
ZnO	33.36	0.94	34.7	4.02	0.50
MgO	13.44	1.39	16.6	23.51	1.75

[a] Average values from the Williamson-Hall, Halder-Wagner, and SSP methods.

application to users.

$$w(2\cot\theta_0 - w) = \frac{1.6\times10^{-3}}{D}\frac{d_0}{w} - \frac{6.2\times10^{-3}}{c} \tag{34}$$

4. Conclusions

In order to determine the behaviour of materials in the nanostructure, it is necessary to explain a model based on a predicted image of the internal structure and demonstrate it as a theoretical approach. The strain is the major factor that redistributes the lattice parameters and hence the intermolecular distances, leading to XRD peak broadening. A novel strain-distribution (SD) model is theoretically built with a peak profile that agrees with the experimental data, and an equation is deduced to calculate the strain exponent and crystalline size. Throughout its methodology, the change in crystal lattice as material is reduced to nanostructure is negated via the strain distribution. The longitudinal strains alone were considered, while the shear strains affect the lattice angles, and their changes were ignored due to the fact that the application of this model to different crystal systems is valid. The well-known Scherrer and Williamson-Hall equations for nanostructures were deduced as approximations of the model, besides showing the reason for negative microstrain. Also, the Halder-Wagner and SSP equations are possible as another approximation. An important part of the SD model is the strain exponent, which plays a big role in the explanation of the reaction of the nanoparticles with the host material. The strain exponent value shows the possibility of aggregates of nanoparticles rather than interactions with the host material. This model is recommended for considering nanostructure studies, especially the interaction of nanoparticles with the host matter.

Ethical approval

No experiments are carried out on human tissues or living organisms by any kind.

Funding declaration

This research received no specific grant from any funding agency in

the public, commercial, or not-for-profit sectors.

CRediT authorship contribution statement

A.S. Abdel-Rahman: Conceptualization, Data curation, Methodology, Writing – original draft, Writing – review & editing. **Youssef A. Sabry:** Conceptualization, Methodology, Writing – original draft.

Declaration of competing interest

The authors declare that they have no known competing financial interests or personal relationships that could have appeared to influence the work reported in this paper.

Data availability

Data will be made available on request.

References

[1] A.S. Abdel-Rahman, Nonlinear Optics, Quantum Optics 57 (3–4) (2023) 175–222.
[2] S.K. Abdel-Aal, et al., J. Phys. Chem. Solid. 161 (2022) 110400, https://doi.org/10.1016/j.jpcs.2021.110400.
[3] S.K. Abdel-Aal, et al., Acta Crystallogr. A73 (2017) C1116, https://doi.org/10.1107/S2053273317084583.
[4] S.K. Abdel-Aal, et al., Acta Crystallogr. B79 (2023) 314–319, https://doi.org/10.1107/S2052520623005309.
[5] S.K. Abdel-Aal, A.S. Abdel-Rahman, J. Cryst. Growth 457 (2017) 282–288, https://doi.org/10.1016/j.jcrysgro.2016.08.006.
[6] S.K. Abdel-Aal, et al., Egypt. J. Solid. 42 (2019/2020) 49–58, https://doi.org/10.21608/EJS.2020.148111.
[7] H. Hassan, et al., Nonlinear Optics Quantum Optics 48 (4) (2018) 313–320.
[8] D. Coetzee, M. Venkataraman, J. Militky, M. Petru, Polymers 12 (4) (2020) 742, https://doi.org/10.3390/polym12040742.
[9] S.M. Bhagyaraj, O.S. Oluwafemi, Ch1-Nanotechnology: the Science of the Invisible, of "Synthesis of Inorganic Nanomaterials", Woodhead Publishing, 2018 https://doi.org/10.1016/B978-0-08-101975-7.00001-4.
[10] S.K. Abdel-Aal, et al., Phys. Status Solidi A218 (12) (2021) 2100036, https://doi.org/10.1002/pssa.202100036.
[11] S.A. Mahmoud, S.M. Al-Shomar, A.A. Akl, Adv. Condens. Matter Phys. 2010 (2010) 518209, https://doi.org/10.1155/2010/518209.
[12] A.A. Akl, A.S. Hassanien, Int. J. Adv. Res. 2 (11) (2014) 1–9.
[13] S.K. Abdel-Aal, A.S. Abdel-Rahaman, J. Nano Res. 22 (9) (2020) 267, https://doi.org/10.1007/s11051-020-05001-7.
[14] A.A. Akl, A.S. Hassanien, Superlattice. Microst. 85 (2015) 67–81, https://doi.org/10.1016/j.spmi.2015.05.011.
[15] A.A. Akl, S.A. Mahmoud, S.M. Al-Shomar, A.S. Hassanien, Mater. Sci. Semicond. Process. 74 (2018) 183–192, https://doi.org/10.1016/j.mssp.2017.10.007.
[16] A.A. Akl, I.M. El Radaf, A.S. Hassanien, Optik 227 (2021) 165837, https://doi.org/10.1016/j.ijleo.2020.165837.
[17] A. Sa'aedi, A.A. Akl, A.S. Hassanien, CrystEngComm 24 (26) (2022) 4661–4678, https://doi.org/10.1039/D2CE00483F.
[18] A.S. Hassanien, I.M. El Radaf, Mater. Sci. Semicond. Process. 160 (2023) 107405, https://doi.org/10.1016/j.mssp.2023.107405.
[19] I.M. El Radaf, A.S. Hassanien, Phys. B Condens. Matter 659 (2023) 414867, https://doi.org/10.1016/j.physb.2023.414867.
[20] A.A.S. Akl, M. Elhadi, J. Ovonic Res. 16 (5) (2020) 323–335.
[21] A.S. Hassanien, A.A. Akl, A.H. Sáaedi, CrystEngComm 20 (12) (2018) 1716–1730, https://doi.org/10.1039/c7ce02173a.
[22] S.K. Abdel-Aal, A.S. Abdel-Rahman, J. Electron. Mater. 48 (3) (2019) 1686–1693, https://doi.org/10.1007/s11664-018-06916-7.
[23] N. Hamdaoui, Y. Azizian-Kalandaragh, B. Zaidi, A.A. Akl, Appl. Phys. A127 (2021) 377, https://doi.org/10.1007/s00339-021-04518-5.
[24] Y.H. Elbashar, et al., Nonlinear Optics Quantum Optics 51 (3–4) (2020) 171–193.
[25] N. Hamdaoui, D. Tlili, Y. Azizian-Kalandaragh, B. Zaidi, S. Zemni, A.A. Akl, L. Beji, J. Mater. Sci. Mater. Electron. 32 (2021) 26984–26997, https://doi.org/10.1007/s10854-021-07072-1.
[26] A.A. Akl, A.S. Hassanien, Phys. B Condens. Matter 620 (2021) 413267, https://doi.org/10.1016/j.physb.2021.413267.
[27] Y.H. Elbashar, et al., Nonlinear Optics Quantum Optics 54 (1–2) (2021) 105–114.
[28] Y.H. Elbashar, et al., Nonlinear Optics Quantum Optics 54 (3–4) (2021) 205–215.
[29] M.F. Kandeel, et al., IOP Conference Series 610 (1) (2019) 012063, https://doi.org/10.1088/1757-899X/610/1/012063.
[30] S.K. Abdel-Aal, et al., Acta Crystallogr. B75 (2019) 880–886, https://doi.org/10.1107/S2052520619011314.
[31] A.S. Abdel-Rahman, Many-body reduced vector solution and water vibrations, Nonlinear Opt. (2024), https://doi.org/10.21203/rs.3.rs-2175055/v2.
[32] S.K. Abdel-Aal, et al., J. Mol. Struct. 1276 (2023) 134757, https://doi.org/10.1016/j.molstruc.2022.134757.
[33] D.I. Moubarak, et al., Nonlinear Optics Quantum Optics 49 (3–4) (2018) 295–310.
[34] D.I. Moubarak, et al., Laser Eng. 43 (4–6) (2019) 201–212.
[35] D.I. Moubarak, et al., Laser Eng. 43 (4–6) (2019) 319–328.
[36] D.I. Moubarak, et al., Nonlinear Optics Quantum Optics 53 (1–2) (2021) 31–59.
[37] Y.H. Elbashar, et al., Nonlinear Optics Quantum Optics 49 (3–4) (2018) 247–265.
[38] Y.H. Elbashar, et al., Annals of the University of Craiova, Physics 28 (2018) 57–72.
[39] Y.H. Elbashar, et al., Nonlinear Optics Quantum Optics 51 (3–4) (2020) 195–212.
[40] Y.H. Elbashar, et al., Nonlinear Optics Quantum Optics 52 (3–4) (2020) 337–347.
[41] Y.H. Elbashar, et al., Nonlinear Optics Quantum Optics 54 (3–4) (2021) 231–239.
[42] A.S. Abdel-Rahman, Y.A. Sabry, Schrödinger Equation and GUP of Attenuated Eigenfunction", *Nonlinear Optics, Quantum Optics: Concepts In Modern Optics*, 2024, https://doi.org/10.22541/au.168067444.49101763/v1.
[43] A.S. Hassanien, A.A. Akl, CrystEngComm 20 (44) (2018) 7120–7129, https://doi.org/10.1039/c8ce01614c.
[44] A.A. Akl, I.M. El Rada, A.S. Hassanien, Superlattice. Microst. 143 (2020) 106544, https://doi.org/10.1016/j.spmi.2020.106544.
[45] S.K. Abdel-Aal, et al., Phys. Status Solidi A218 (12) (2021) 2100138, https://doi.org/10.1002/pssa.202100138.
[46] N.S. Pillai, X.-L. Meng, Ann. Stat. 44 (5) (2016) 2089–2097, https://doi.org/10.1214/15-AOS1407.
[47] M. Norton, V. Khokhlov, S. Uryasev, Ann. Oper. Res. 299 (2021) 1281–1315, https://doi.org/10.1007/s10479-019-03373-1.
[48] A.S. Abdel-rahman, Int. J. Comput. Methods Eng. Sci. Mech. 24 (2) (2023) 155–166, https://doi.org/10.1080/15502287.2022.2113184.
[49] I. Hammami, N.M. Alabdallah, A. Al jomaa, M. Kamoun, J. King Saud Univ. Sci. 33 (7) (2021) 101560, https://doi.org/10.1016/j.jksus.2021.101560.
[50] R. Sivakami, et al., Spectrochim. Acta Mol. Biomol. Spectrosc. 152 (2016) 43–50.
[51] K. Maniammal, et al., Physica E85 (2017) 214–222.
[52] A.K.M. Atique Ullah, A.K.M. Fazle Kibria, M. Akter, M.N.I. Khan, A.R.M. Tareq, S. H. Firoz, Water Cons. Sci. Engin. 1 (2017) 249–256, https://doi.org/10.1007/s41101-017-0017-3.
[53] S. Sankadiya, et al., AIP Conf. Proc. 1724 (2016) 020064.
[54] V.N. Kalpana, B.A.S. Kataru, N. Sravani, T. Vigneshwari, A. Panneerselvam, V. D. Rajeswari, OpenNano 3 (2018) 48–55, https://doi.org/10.1016/j.onano.2018.06.001.
[55] G. Balakrishnan, et al., Res. Phys. 16 (2020) 103013.
[56] C.S. Joshi, R.C. Srivastava, A. Joshi, M. Tiwari, J. Mater. Sci. Mater. Electron. 34 (2023) 2097, https://doi.org/10.1007/s10854-023-11515-2.